Solution Conformation of the (−)-*trans-anti*-Benzo[*c*]phenanthrene-dA ([BPh]dA) Adduct opposite dT in a DNA Duplex: Intercalation of the Covalently Attached Benzo[*c*]phenanthrenyl Ring to the 3′-Side of the Adduct Site and Comparison with the (+)-*trans-anti*-[BPh]dA opposite dT Stereoisomer†

Monique Cosman,‡ Alfred Laryea,§ Radovan Fiala,‡ Brian E. Hingerty,|| Shantu Amin,⊥ Nicholas E. Geacintov,§ Suse Broyde,# and Dinshaw J. Patel*,‡

Cellular Biochemistry and Biophysics Program, Memorial Sloan-Kettering Cancer Center, New York, New York 10021, Chemistry and Biology Departments, New York University, New York, New York 10003, Health Sciences Research Division, Oak Ridge National Laboratory, Oak Ridge, Tennessee 37831, and American Health Foundation, Valhalla, New York 10595

Received August 24, 1994; Revised Manuscript Received November 10, 1994®

ABSTRACT: This paper reports on NMR−molecular mechanics structural studies of the (−)-*trans-anti*-benzo[*c*]phenanthrene-dA adduct positioned opposite dT in the sequence context of the d(C1-T2-C3-T4-C5-[BPh]A6-C7-T8-T9-C10-C11)·d(G12-G13-A14-A15-G16-T17-G18-A19-G20-A21-G22) duplex (designated as the (−)-*trans-anti*-[BPh]dA·dT 11-mer duplex). This adduct is derived from the covalent binding of (−)-1,2-dihydroxy-3,4-epoxy-1,2,3,4-tetrahydro-benzo[*c*]phenanthrene [(−)-*anti*-BPhDE] to N^6 of dA6 in this duplex sequence. The benzo[*c*]phenanthrenyl and nucleic acid exchangeable and nonexchangeable protons were assigned in the predominant conformation following analysis of two-dimensional NMR data sets in H_2O and D_2O buffer solution. The solution structure of the (−)-*trans-anti*-[BPh]dA·dT 11-mer duplex has been determined by incorporating intramolecular and carcinogen−DNA proton−proton distances defined by lower and upper bounds deduced from NOESY data sets as restraints in molecular mechanics computations in torsion angle space. The results show that the [BPh]dA6·dT17 base pair propeller twists and buckles slightly to permit the covalently attached benzo[*c*]phenanthrenyl ring to intercalate between the [BPh]dA6·dT17 and dC7·dG16 base pairs to the 3′-side of the [BPh]dA6 lesion site without disrupting the Watson−Crick hydrogen bond alignments in the modified duplex. The strain in the highly sterically hindered fjord region of the benzo[*c*]phenanthrenyl moiety is relieved by the propeller-like nonplanar geometry of the aromatic phenanthrenyl ring system, which stacks predominantly with the dG16 and dT17 bases on the unmodified strand. The benzylic ring adopts a distorted half-chair form, in which the H1 and H2 protons are pseudo-diequatorial and the H3 and H4 protons are pseudo-diaxial. The current observation that the (−)-*trans-anti*-[BPh]dA positioned opposite dT intercalates to the 3′-side of the intact modified base pair contrasts with our previous demonstration that the stereoisomeric (+)-*trans-anti*-[BPh]dA adduct positioned opposite dT intercalates to the 5′-side of the intact modified base pair [Cosman, M., et al. (1993b) *Biochemistry 32*, 12488−12497]. These stereochemically induced structural differences between isomeric [BPh]dA lesions derived from the binding of chiral (+)- and (−)-*anti*-BPhDE enantiomers may in turn profoundly influence the interactions of the carcinogen-modified DNA with repair and replication enzymes in the cell.

Polycyclic aromatic hydrocarbons (PAH) are byproducts of fossil fuel combustion and therefore are ubiquituous in our environment (Lunde & Bjoresth, 1977; Wise et al., 1986). Many of these environmental contaminants are metabolically activated to highly reactive, mutagenic and carcinogenic PAH diol epoxide derivatives [reviewed in Miller (1978); Singer & Grunberger, 1983; Harvey, 1991], and the parent PAH compounds therefore constitute a significant potential health hazard (Grimmer, 1993). The role of stereochemistry in the metabolic activation of compounds to diol epoxide derivatives is well established (Conney, 1982). The covalent binding of the diol epoxide derivatives to native DNA gives rise to mutations and is believed to initiate the complex, multistage carcinogenic process (Harris, 1991). Chiral effects governing the mechanisms of binding and the structural features of the covalent PAH diol epoxide−DNA adducts formed (Cosman et al., 1992, 1993a,b; De los Santos et al., 1992; Singh et al., 1991) are critical factors that can influence the adverse biological effects associated with each stereoisomer.

The ultimate tumorigenic and mutagenic metabolites of the weakly tumorigenic parent benzo[*c*]phenanthrene are the fjord region epoxides 3,4-dihydroxy-1,2-epoxy-1,2,3,4-tetrahydrobenzo[*c*]phenanthrenes (BPhDE) (Levin et al., 1980; Jerina et al., 1984; Wood et al., 1984; Thakker et al., 1986; Pruess-Schwartz et al., 1987). The fjord region designation refers to the severely sterically hindered region between C^1

† This research is supported by NIH Grant CA-46533 to D.J.P., NIH Grant CA-20851 and DOE Grant DE-FG02-88ER60405 to N.E.G., NIH Grants CA-28038 and RR-06458 and DOE Grant DE-FG02-90ER60931 to S.B., and DOE Contract DE-AC05-840R21400 with Martin-Marietta Energy Systems and DOE OHER Field Work Proposal ERKP931 to B.E.H.

‡ Memorial Sloan-Kettering Cancer Center.
§ Chemistry Department, New York University.
|| Oak Ridge National Laboratory.
⊥ American Health Foundation.
Biology Department, New York University.

® Abstract published in *Advance ACS Abstracts,* January 15, 1995.

0006-2960/95/0434-1295$09.00/0

on the benzylic ring and C^{12} on the vicinal phenanthrene ring (Levin et al., 1980). BPhDE can be synthesized as a pair of diastereoisomers, labeled *syn*- or *anti*-diol epoxide, respectively, in which the hydroxyl at the 4-position can be either *syn* or *anti* to the oxirane oxygen, and each diastereoisomer in turn can be further resolved into two enantiomers, designated (+) and (−) (Yagi et al., 1983). All four BPhDE stereoisomers react extensively with both guanine and adenine residues in native DNA *in vitro* (Levin et al., 1980; Dipple et al., 1987; Agarwal et al., 1987; Bigger et al., 1989; Canella et al., 1992) and in rodent embryo cell cultures (Pruess-Schartz et al., 1987).

All four BPhDE stereoisomers are mutagenic (Wood et al., 1984; Bigger et al., 1989, 1992) and tumorigenic (Levin et al., 1986), and the relative extent of biological activity observed is system dependent. In histidine dependent strains in *Salmonella typhimurium*, (−)-*anti*-BPhDE was found to be 2−4-fold less active in generating mutations than the enantiomeric (+)-*anti* isomer, while it was the most active stereoisomer in 8-azaguanine sensitive Chinese hamster V79 cells (Wood et al., 1984). On mouse skin, both the (−)-*anti*- and (+)-*syn*-BPhDE stereoisomers are twice as active as the (+)-*anti* isomer (Levin et al., 1986). However, in newborn mice, (−)-*anti*-BPhDE was almost 10-fold more active in producing lung tumors than the next most active compound, (+)-*anti*-BPhDE (Levin et al., 1986). In addition, at high doses, only the (−)-*anti*-BPhDE isomer produced a significant number of hepatic tumors, and this compound was found to be the most tumorigenic bay region diol epoxide tested to date in newborn mice (Levin et al., 1986). More recently, racemic *anti*-BPhDE has been shown to be a powerful rat mammary gland tumorigen as well (Hecht et al., 1994).

Using high-resolution NMR and computational methods, we have recently reported on the solution structures of stereoisomeric benzo[*a*]pyrenylguanine ([BP]-N^2-dG) adducts positioned opposite dC and the deletion sites at the DNA duplex level in which the covalent binding site is located along the minor groove edge. The pyrenyl moiety of the [BP]dG adduct positioned opposite dC was either situated in the minor groove without disruption of the modified base pair [(+)- and (−)-*trans-anti* stereoisomers] (Cosman et al., 1992; De los Santos et al., 1992) or intercalated into the helix following disruption and displacement of the modified base pair [(+)-*cis-anti* isomer] (Cosman et al., 1993a). The pyrenyl moiety of the [BP]dG adduct intercalates into the helix when positioned opposite deletion sites, with base displacement of the modified guanine base into either the major groove [(+)-*trans-anti* isomer] (Cosman et al., 1994a) or the minor groove [(+)-*cis-anti* isomer] (Cosman et al., 1994b).

These NMR−molecular mechanics studies have recently been extended to benzo[*c*]phenanthrenyladenine ([BPh]-N^6-dA) adducts positioned opposite dT at the DNA duplex level, in which the covalent binding site is located along the major groove edge. We recently reported on the solution structure of the (+)-*trans-anti*-[BPh]dA adduct positioned opposite dT in the d(C-[BPh]A-C)·d(G-T-G) sequence context and established a wedge-shaped intercalation complex, in which the phenanthrenyl ring is inserted into the 5′-side of the modified adenine without disruption of the [BPh]dA·dT base pair (Cosman et al., 1993b). In the present paper, we have used a combined two-dimensional NMR−molecular mechanics approach to determine the solution structure of the stereoisomeric (−)-*trans-anti*-[BPh]dA adduct (**1**) positioned opposite dT in the same sequence context at the duplex level [designated (−)-*trans-anti*-[BPh]dA·dT 11-mer duplex (**2**)], in which the modification site is flanked by dG·dC base pairs. Our results establish that the covalently attached benzo[*c*]-phenanthrenyl ring intercalates to the 3′-side of the (−)-*trans-anti*-[BPh]dA adduct site, in a direction opposite that found in the solution structure of the (+)-*trans-anti* stereoisomer (Cosman et al., 1993b).

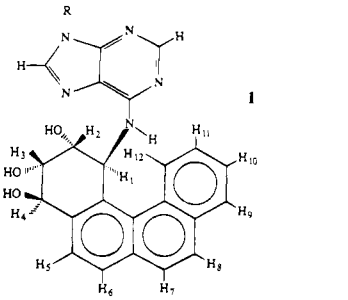

1

C1-T2-C3-T4-C5-A6-C7-T8-T9-C10-C11

G22-A21-G20-A19-G18-T17-G16-A15-A14-G13-G12

2

MATERIALS AND METHODS

Preparation of the (−)-trans-anti-[BPh]dA·dT 11-mer Duplex. Racemic *anti*-BPhDE was synthesized according to the published procedures (Misra & Amin, 1990). The synthesis of the [BPh]dA covalent adducts in the d(C-T-C-T-C-A-C-T-T-C-C) sequence was carried out starting with racemic *anti*-BPhDE using previously described methods (Cosman et al., 1990, 1993b). The (−)-*trans-anti*-[BPh]dA-containing 11-mer was separable from the (+)-*trans-anti* stereoisomer by preparative HPLC on a C18 ODS Hypersil column. In order to establish the identity of the adduct, the modified oligomer strand was degraded with spleen exonuclease (phosphodiesterase II, Worthington Biochemical Corp., Freehold, NJ), as described by Razzel and Khorana (1961), to the 2′-deoxyribonucleosides. The base composition of the modified oligomer was characterized and verified using methods described by Agarwal et al. (1987) and Dipple et al. (1987) using CD and UV absorption spectroscopy. The synthesis and characterization of these adducts will be fully described elsewhere (A. Laryea, M. Cosman, J. Liu, P. M. Liu, R. Agarwal, S. Smirov, S. Amin, R. G. Harvey, A. Dipple, and N. E. Geacintov, manuscript in preparation). The modified stereoisomerically pure d(C-T-C-T-C-[BPh]A-C-T-T-C-C) strand was annealed to its complementary unmodified d(G-G-A-A-G-T-G-A-G-A-G) strand at 70 °C, and the stoichiometry was followed by monitoring single proton resonances in both strands. The sample concentration was 1.7 mg of modified duplex in 0.6 mL of 0.1 M NaCl/10 mM phosphate aqueous buffer (pH 7.0).

NMR Experiments. A combination of through-space nuclear Overhauser effect (NOESY) and through-bond correlated (COSY and TOCSY) two-dimensional spectra was recorded and analyzed to assign the carcinogen and nucleic acid protons in the (−)-*trans-anti*-[BPh]dA·dT 11-mer duplex. All experiments were carried out using a Varian Unity

Plus 600 MHz instrument in the States-TPPI mode (Marion et al., 1989), with a 2.0 s relaxation delay between scans. The temperature of the sample was calibrated with an external methanol sample. The NOESY spectrum (150 ms mixing time) was collected on the modified duplex in H_2O buffer at 1 °C using a jump−return pulse for solvent suppression, and NOESY spectra (40, 50, 80, 120, 160, 200, and 300 ms mixing times) were recorded in D_2O buffer at 25 °C. The through-bond TOCSY data sets in D_2O buffer at 25 °C were recorded at spin-lock times of 40 and 80 ms. The proton−phosphorus correlation spectra of the modified duplex in D_2O buffer at 25 °C were recorded using the method described in Sklenar et al. (1986), with sweep widths set to 6 ppm in both ω_1 and ω_2, and with a 1.3 s presaturation of the HDO signal. An external 10% (v/v) trimethyl phosphate sample was used to reference the phosphorus spectra.

Several factors went into the conversion of the NOE intensities into the distance bounds used for the structure determination. The volume integrals of nonexchangeable proton cross peaks of the adduct duplex in D_2O buffer were measured as a function of five mixing times (40, 80, 120, 160, and 200 ms) to generate the buildup curves. The interproton distance calculations were based on the isolated two-spin approximation using the dT(NH3)−dA(H2) fixed distance of 2.92 Å for the NOESY spectrum in H_2O and the dC(H6)−dC(H5) fixed distance of 2.45 Å for the NOESY data sets in D_2O solution. The choice of upper and lower bound ranges for the estimated distances depended on the resolution of the cross peaks in the two-dimensional contour plots. The base proton to sugar H1′ NOE cross peaks in the shortest mixing time NOESY data set in D_2O were evaluated to qualitatively differentiate between *syn* (strong NOE) and *anti* (weak NOE) glycosidic torsion angles (Patel et al., 1982).

The proton−proton vicinal coupling constants among sugar protons were analyzed from phase sensitive COSY spectra to qualitatively distinguish between the C3′-*endo* and C2′-*endo* family of sugar puckers in the (−)-*trans-anti*-[BPh]-dA·dT 11-mer duplex. The relative intensities of the NOE cross peaks between base protons and their own and 5′-flanking sugar H2′, H2″, and H3′ protons were also used to qualitatively distinguish between the A and B family of helices for the modified duplex (van der Ven & Hilbers, 1988). The proton−proton vicinal coupling constant patterns in the benzylic ring of the [BPh]dA adduct were computed using the SPHINX and LINSHA programs (K. Wuthrich, ETH, Zurich) and with the program CHORDS (Majumdar & Hosur, 1992) to constrain torsion angles linking the BPh(H1)−BPh(H2) and BPh(H3)−BPh(H4) proton pairs.

Molecular Mechanics Computations. Minimized potential energy calculations were carried out with DUPLEX, a molecular mechanics program for nucleic acids that performs potential energy minimizations in the reduced variable domain of torsion angle space (Hingerty et al., 1989). The advantage of torsion space, compared to Cartesian space minimizations, is the vast diminution in the number of variables that must be simultaneously optimized, thereby permitting larger movements from a given starting conformation during minimization, as well as assurance of realistic internal geometry.

DUPLEX uses a potential set similar to the one developed by Olson and co-workers for nucleic acids (Taylor & Olson, 1983) for which details have been published previously (Hingerty et al., 1989). Force field parameters, including partial charges, for the (−)-*trans-anti*-[BPh]dA adduct were the same as those employed for the (+)-*trans-anti*-[BPh]dA adduct (Cosman et al., 1993b). A hydrogen bond penalty function (Hingerty et al., 1989) was employed in all first-stage minimizations to aid the minimizer in locating the Watson−Crick hydrogen-bonded structures indicated by the NMR data. To locate minimum energy conformations with interproton distances suggested from the experimental NMR data, pseudopotentials (permitting upper and lower bound restraints) were added to the energy, as described previously (Norman et al., 1989; Schlick et al., 1990). Briefly, the following functions were used:

$$F_N = W_N \sum_1^n (d - d_N)^2 \quad (1)$$

$$F_{NN} = W_{NN} \sum_1^n (d - d_{NN})^2 \quad (2)$$

The W's are adjustable weights (in the range of 10−30 kcal/mol·Å^2), d is the current value of the interproton distance, d_N is a target upper bound, and d_{NN} is a target lower bound. The summation is over all n NMR-derived distance bounds. Equation 1 is implemented when d is greater than d_N, and eq 2 is implemented when d is less than d_{NN}. F_N and F_{NN} can also be employed as goodness-of-fit indices to compare the quality of computed structures with respect to the NMR data. In this case d is the distance achieved in the model. All penalty functions were released in the last minimization steps to yield unrestrained final structures that are energy minima.

The geometry (bond lengths, bond angles, and dihedral angles) of the (−)-*trans-anti*-[BPh]dA adduct was generated as follows: The adduct was created by computer graphics on a Silicon Graphics Crimson computer with the program INSIGHTII (Biosym Technologies, Inc., Parsippany, NJ). A distorted half-chair form with the BPh(H1) and BPh(H2) protons in the diequatorial domain and the BPh(H3) and BPh(H4) protons in the diaxial domain (Neidle et al., 1982) was employed for the conformation of the benzylic ring, as the simulation of the COSY cross peaks (see Results section) had shown this to be the correct orientation. The constructed model was energy minimized with MACROMODEL V3.5x (Mohamadi et al., 1990), using the Macromodel implementation of the MM3 force field (MM3*) with the solvent and extended nonbonded cutoff options. The resulting structure was then implemented within DUPLEX.

Computations were carried out at the Department of Energy's National Energy Research Supercomputer Center and the National Science Foundation's San Diego Supercomputer Center.

RESULTS

Exchangeable Nucleic Acid Protons. The exchangeable proton NMR spectrum (7.0−15.0 ppm) of the (−)-*trans-anti*-[BPh]dA·dT 11-mer duplex in H_2O buffer (pH 7.0) at 1 °C is plotted in Figure 1A. The exchangeable imino protons of the major species resonate between 11 and 14 ppm, along with resonances from one (or more) minor species also detected in this spectrum (Figure 1A). This

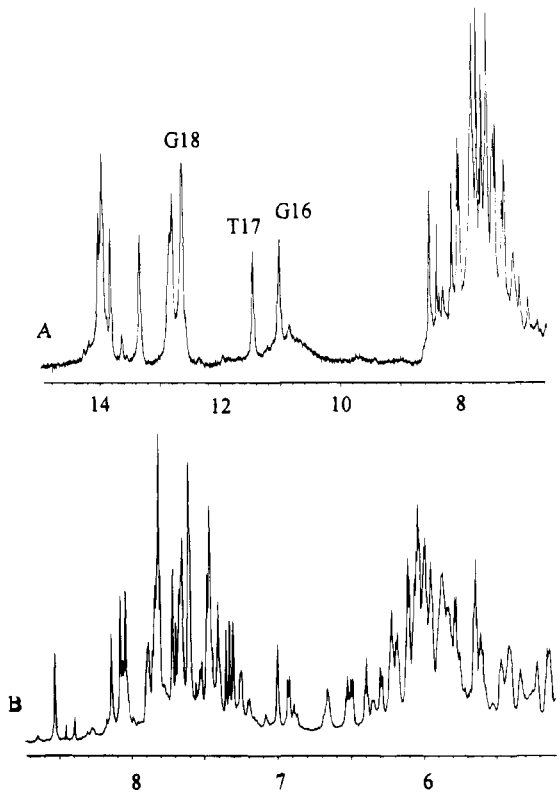

FIGURE 1: (A) Exchangeable proton spectrum (6.0−15.0 ppm) in H_2O buffer at 1 °C and (B) nonexchangeable proton spectrum (5.2−8.7 ppm) in D_2O buffer at 25 °C of the (−)-*trans-anti*-[BPh]dA•dT 11-mer duplex. The buffer was 0.1 M NaCl/10 mM phosphate/0.1 mM EDTA, aqueous solution, pH 7.0. Selective imino proton assignments are recorded over the spectrum in (A).

paper focuses on defining the conformation of the major species of the (−)-*trans-anti*-[BPh]dA•dT 11-mer duplex. Two exchangeable protons at 11.04 and 11.48 ppm are detected that resonate upfield of the normal hydrogen-bonded imino proton spectral region. The imino protons have been assigned following analysis of the 150 ms mixing time NOESY spectrum of the adduct duplex in H_2O buffer solution at 1 °C. The presence of NOE cross peaks between imino protons on adjacent base pairs along the length of the modified duplex can be monitored and traced in the expanded NOESY contour plot of the symmetrical 10.5−14.5 ppm region in Figure 2A. This tracing for the imino protons of the central d(T4-C5-[BPh]A6-C7-T8)•d(A15-G16-T17-G18-A19) segment is shown in Figure 2A and can be readily followed, except for a missing NOE (see box, Figure 2A) between the upfield-shifted imino protons of dT17 (11.48 ppm) and dG16 (11.15 ppm).

An expanded NOESY contour plot (150 ms mixing time) correlating the NOEs between the imino protons (10.5−14.5 ppm) and the amino protons (5.0−9.0 ppm) in the adduct duplex is plotted in Figure 2B. The observed NOE patterns establish Watson−Crick pairing at all six dG•dC pairs (guanine imino to cytosine amino NOE connectivities), as shown for the dC5•dG18 (peaks A and A′, Figure 2B) and dC7•dG16 pairs (peaks B and B′, Figure 2B), which flank the lesion site. The observed NOE patterns also establish Watson−Crick pairing at all four unmodified dA•dT pairs (thymine imino to adenine H2 NOE connectivities). More significantly, the imino proton of dT17 shows medium intensity NOEs to the H2 and NH6 amino protons of [BPh]-dA6 (peaks D and C, respectively, Figure 2B) across the

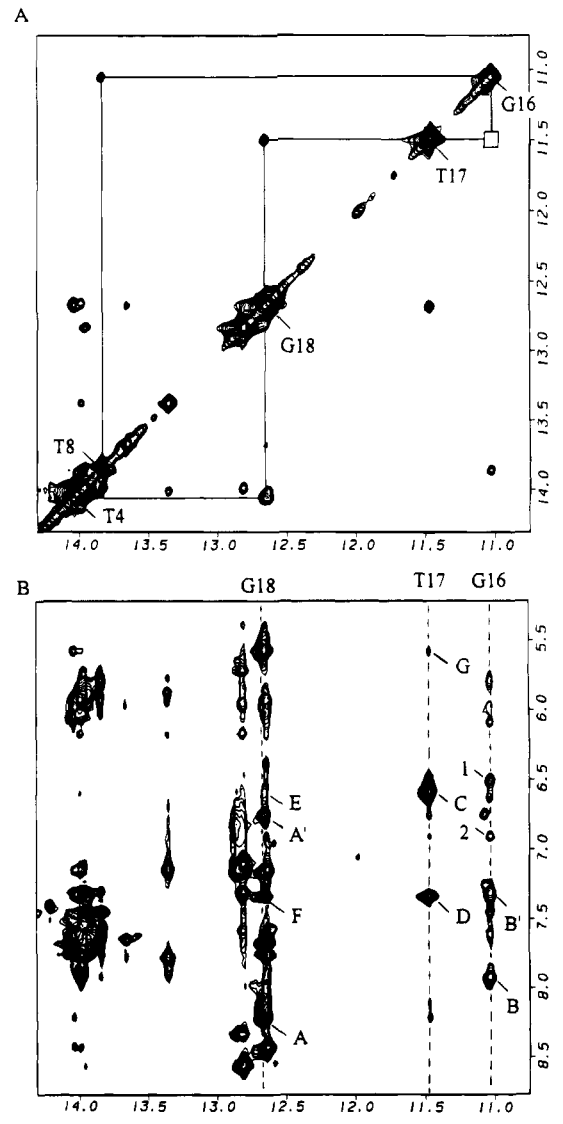

FIGURE 2: Expanded NOESY (150 ms mixing time) contour plots of the (−)-*trans-anti*-[BPh]dA•dT 11-mer duplex in H_2O buffer at 1 °C. (A) NOE connectivities in the symmetrical 10.8−14.3 ppm region. The imino assignments of the central d(T4-C5-[BPh]A6-C7-T8)•d(A15-G16-T17-G18-A19) segment are labeled along the diagonal. The lines trace the NOE connectivities between adjacent base pairs, starting at T4 toward one end of the helix and proceeding to T8 toward the other end of the helix. Note that no NOE connectivity is detected between the imino protons of adjacent dG16 and dT17 (boxed region). (B) NOE connectivities between the imino protons (10.8−14.3 ppm) and the nucleic acid base and amino protons and BPh protons (5.2−8.8 ppm). The NOE cross peaks involving the amino protons of dG16, dT17, and dG18 centered about the lesion site are labeled in the figure. The cross peaks A−G are assigned as follows: A, A′, dG18(NH1)−dC5(NH_2-4b,e); B, B′, dG16(NH1)−dC7(NH_2-4b,e); C, dT17(NH3)−dA6(NH6); D, dT17(NH3)−[BPh]dA6(H2); E, dG18(NH1)−[BPh]dA6(NH6); F, dG18(NH1)−[BPh]dA6(H2); G, dT17(NH3)−dC5(H5). The carcinogen−DNA NOEs numbered 1 and 2 are assigned as follows: 1, dG16(NH1)−BPh(H8) and/or −BPh(H10); 2, dG16-(NH1)−BPh(H9).

pair, establishing the formation of an intact Watson−Crick [BPh]dA6•dT17 base pair at the lesion site. In addition, the dG18 imino proton shows NOEs to the minor groove H2 proton of [BPh]dA6 (medium intensity peak F, Figure 2B) and to the major groove NH6 proton of [BPh]dA6 (weak intensity peak E, Figure 2B), establishing that the dC5•dG18 and [BPh]dA6•dT17 base pairs are stacked on each other. By contrast, NOEs between exchangeable protons on [BPh]-

Table 1: Proton Chemical Shifts of the d(C5-[BPh]A6-C7)•d(G16-T17-G18) Segment of the (−)-*trans-anti*-[BPh]dA•dT 11-mer Duplex in Aqueous Buffer

Exchangeable Proton Chemical Shifts (ppm, 1 °C)				
	G(NH1)	T(NH3)	C(NH_2-4)	A(NH_2-6)
dC5•dG18	12.67		6.75,[a] 8.21[b]	
[BPh]dA6•dT17		11.48		6.58
dC7•dG16	11.04		7.31,[a] 7.92[b]	

Nonexchangeable Proton Chemical Shifts (ppm, 25 °C)						
	H8/H6	H2/H5/CH_3	H1′	H2′, H2″	H3′	H4′
dC5	7.43	5.64	4.78	1.77, 1.70	4.68	3.96
[BPh]dA6	8.52	7.31	6.39	3.02, 2.90	5.20	4.44
dC7	7.83	6.10	5.99	2.29, 2.44	4.87	4.27
dG16	7.39		5.64	2.59, 2.59	5.01	4.28
dT17	6.98	1.30	5.32	1.88, 2.14	4.69	4.10
dG18	7.81		5.14	2.68, 2.63	4.92	4.22

[a] Exposed amino proton. [b] Hydrogen-bonded amino proton.

dA6•dT17 and dC7•dG16 are not detected (see box, Figure 2A), although these base pairs are also adjacent to each other in the sequence of the modified duplex.

The exchangeable imino and amino proton chemical shifts for the central d(C5-[BPh]A6-C7)•d(G16-T17-G18) segment of the adduct duplex are listed in Table 1. The exchangeable proton chemical shift assignments for the entire adduct duplex are listed in Table S1 of the supplementary material.

Nonexchangeable Nucleic Acid Protons. The proton NMR spectrum (5.0−9.0 ppm) of the (−)-*trans-anti*-[BPh]dA•dT 11-mer duplex in D_2O buffer (pH 7.0) at 25 °C is plotted in Figure 1B. The nonexchangeable base and sugar H1′ protons of the major species are well resolved in this spectrum. An expanded NOESY (300 ms mixing time) contour plot correlating the base protons (6.4−8.6 ppm) and the sugar H1′ protons (4.5−6.4 ppm) of the (−)-*trans-anti*-[BPh]dA•dT 11-mer duplex at 25 °C is plotted in Figure 3. By using sequential NOEs between the base (purine H8 or pyrimidine H6) protons and their own and 5′-flanking sugar H1′ protons (Hare et al., 1983), the chain is traced from dT4 to dT8 on the modified strand and from dA15 to dA19 on the unmodified complementary strand, with a loss of connectivity occurring at the dC5-[BPh]dA6 step on the modified strand (box b, Figure 3) and at the dG16-dT17 step on the unmodified complementary strand (box c, Figure 3). These base and sugar H1′ proton assignments have been confirmed by cross-checks in other regions of the NOESY plot, as well as from an analysis of COSY and TOCSY plots to yield a complete set of sugar H2′, H2″, H3′, and H4′ proton assignments. The nonexchangeable proton chemical shifts for the central d(C5-[BPh]A6-C7)•d(G16-T17-G18) segment in the adduct duplex are listed in Table 1. The nonexchangeable base and sugar proton chemical shift assignments for the entire adduct duplex are listed in Table S2 of the supplementary material.

The proton chemical shift differences between the adduct duplex and the unmodified control duplex are given in Table S3 of the supplementary material. Relative to the control duplex, large upfield chemical shift differences are observed for the imino protons of dG16 (−1.68 ppm) and dT17 (−2.04 ppm) in the adduct duplex. A moderate upfield chemical shift is also observed for the dC5 exposed amino proton (−0.77 ppm), while the exposed amino proton of dC7 shifts downfield (+0.63 ppm) upon adduct formation. Also upon adduct formation, upfield chemical shifts are observed for

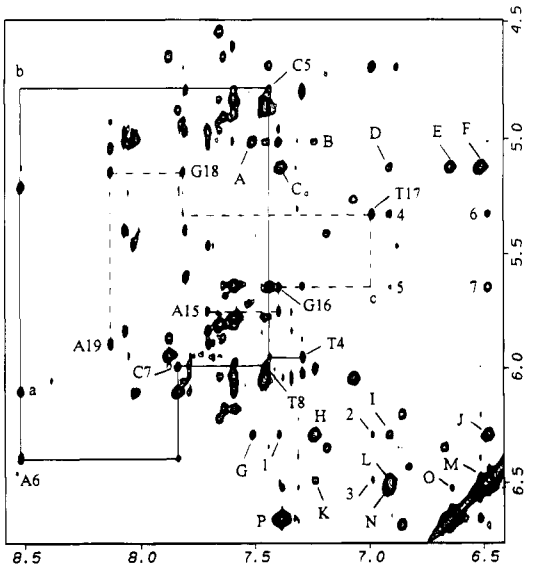

FIGURE 3: Expanded NOESY (300 ms mixing time) contour plot of the (−)-*trans-anti*-[BPh]dA•dT 11-mer duplex in D_2O buffer at 25 °C, establishing distance connectivities between the base (purine H8 and pyrimidine H6) protons (6.4−8.6 ppm) and the sugar H1′ and cytosine H5 protons (4.5−6.8 ppm). The NOE connectivities between the bases and their own and 5′-flanking sugar H1′ protons are traced from dT4 to dT8 on the modified strand (solid line) and from dA15 to dA19 on the unmodified strand (dashed line). The cross peak between the [BPh]dA6(H8) and dC7(H5) protons is designated a, and the missing cross peaks between dC5(H1′) and [BPh]dA6(H8) and between dG16(H1′) and dT17(H6) are designated by boxes labeled b and c, respectively. The cross peaks labeled A−P identify NOEs among benzo[*c*]phenanthrenyl protons and are assigned as follows: A, BPh(H4)−BPh(H5); B, BPh(H4)−BPh(H6); C, BPh(H11)−BPh(H12); D, BPh(H11)−BPh(H9); E, BPh(H11)−BPh(H1); F, BPh(H11)−BPh(H10); G, BPh(H7)−BPh(H5); H, BPh(H7)−BPh(H6); I, BPh(H7)−BPh(H9); J, BPh(H7)−BPh(H8); K, BPh(H8)−BPh(H6); L, BPh(H8)−BPh(H9); M, BPh(H10)−BPh(H12); N, BPh(H10)−BPh(H9); O, BPh(H10)−BPh(H1); P, BPh(H1)−BPh(H12). The cross peaks numbered 1−7 identify carcinogen−DNA NOEs and are assigned as follows: 1, BPh(H7)−dG16(H8); 2, BPh(H7)−dT17(H6); 3, BPh(H8)−dT17(H6); 4, BPh(H9)−dT17(H1′); 5, BPh(H9)−dG16(H1′); 6, BPh(H8)−dT17(H1′); 7, BPh(H8)−dG16(H1′).

the dC5(H1′) (−0.63 ppm), dC5(H2″) (−0.64 ppm), and dG18(H1′) (−0.26 ppm) minor groove sugar protons of the dC5•dG18 base pair located 5′ to the lesion site. By contrast, downfield shifts are observed for the dC7(H5) (+0.88 ppm), dC7(H6) (+0.57 ppm), dC7(H2′) (+0.32 ppm), dC7(H3′) (+0.23 ppm), and dG16(H2′) (+0.24 ppm) major groove base and sugar protons of the dC7•dG16 base pair located 3′ to the lesion site.

We detected an NOE between the [BPh]dA6(H8) proton and the 3′-side major groove dC7(H5) base proton (peak a, Figure 3), while no NOE is detected between the [BPh]dA6(H8) proton and the 5′-side minor groove dC5(H1′) sugar proton (box b, Figure 3), indicating that the major groove edge of the modified adenine of [BPh]dA6 is tipping toward the 3′-side major groove edge of the dC7 residue.

Nonexchangeable Benzo[c]phenanthrenyl Protons. The nonexchangeable benzo[*c*]phenanthrenyl protons were assigned from an analysis of the through-bond and through-space connectivities in the (−)-*trans-anti*-[BPh]dA•dT 11-mer duplex. Their chemical shifts in the adduct duplex are listed in the caption to Figure 4. The aromatic phenanthrenyl protons are all shifted upfield in the (−)-*trans-anti*-[BPh]-

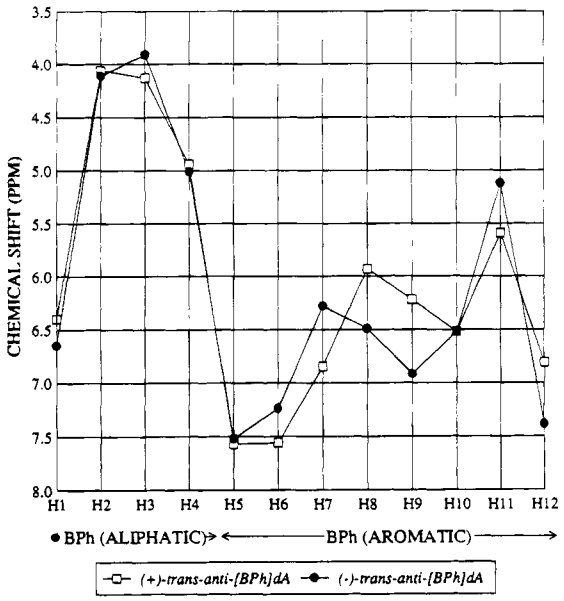

FIGURE 4: Plot comparing the benzo[*c*]phenanthrenyl ring proton chemical shifts in the (−)-*trans-anti*-[BPh]dA•dT 11-mer and (+)-*trans-anti*-[BPh]dA•dT 11-mer duplexes in D_2O buffer at 25 °C. The chemical shift values in ppm for the phenanthrenyl protons in the (−)-*trans-anti*-[BPh]dA isomer are as follows: BPh(H1), 6.65; BPh(H2), 4.11; BPh(H3), 3.91; BPh(H4), 5.01; BPh(H5), 7.52; BPh(H6), 7.24; BPh(H7), 6.28; BPh(H8), 6.49; BPh(H9), 6.92; BPh(H10), 6.52; BPh(H11), 5.12; BPh(H12), 7.39.

dA•dT 11-mer duplex relative to their values (8.0 and 8.5 ppm) in protected [BPh]dA nucleotide adducts (Agarwal et al., 1987). In particular, H7, H8, H10, and H11 are shifted by more than 1.5 ppm to high field. A graph comparing the chemical shifts of the BPh protons in the (−)-*trans-anti*-[BPh]dA•dT 11-mer duplex (present work) with those of the BPh protons in the stereoisomeric (+)-*trans-anti*-[BPh]dA•dT 11-mer duplex (Cosman et al., 1993b) is shown in Figure 4. The same trend in upfield shifts is detected for the phenanthrenyl protons in both adduct duplexes, independent of the chirality [(+)-*trans-anti* or (−)-*trans-anti*] of the [BPh]dA stereoisomer.

The experimental coupling cross peaks BPh(H1)−BPh(H2) and BPh(H3)−BPh(H4) are well resolved, while the BPh(H2)−BPh(H3) cross peak is located close to the diagonal in an overlapped region of the phase sensitive COSY spectrum of the adduct duplex. There is good agreement between the experimental coupling cross-peak patterns and their simulated counterparts based on three-bond vicinal proton−proton coupling constant values of ^3J(H1,H2) = 4.4 ± 0.2 Hz, ^3J(H2,H3) = 4.0 ± 0.5 Hz, and ^3J(H3,H4) = 6.5 ± 0.5 Hz. These vicinal coupling constant values are consistent with the distorted half-chair conformation of the benzylic ring, where the BPh(H1) and BPh(H2) protons adopt pseudo-diequatorial orientations while the BPh(H3) and BPh(H4) protons adopt pseudo-diaxial orientations.

Carcinogen−DNA NOEs. An NOE data set distributed between 5 exchangeable BPh−DNA protons and 22 non-exchangeable BPh−DNA protons was used to define the distance restraints for the (−)-*trans-anti*-[BPh]dA•dT 11-mer duplex (Table 2). Several of the carcinogen−DNA NOEs are labeled by numbers in the expanded NOESY (150 ms mixing time) contour plot of exchangeable protons in H_2O solution (Figure 2B and Figure S1 of the supplementary material) and in the expanded NOESY (300 ms mixing time) contour plots of nonexchangeable protons in D_2O buffer (Figures 3 and 5). The carcinogen−DNA NOE cross-peak assignments are listed in the figure captions. The corresponding carcinogen−DNA distance restraints defined by lower and upper bounds for the central d(C5-[BPh]A6-C7)•d(G16-T17-G18) segment, together with five additional important DNA−DNA distance restraints that define the position of the modified adenine of [BPh]dA6 in the DNA helix, are listed in Table 2.

Table 2: Comparison of Input Interproton Distance Bounds with Those Observed for the NMR Energy-Minimized Solution Structure of the (−)-*trans-anti*-[BPh]dA•dT 11-mer Duplex

	interproton distances (Å)	
	experimental bounds	observed
Exchangeable Protons (DNA−DNA)		
[BPh]dA6(NH6)−dG18(NH1)	4.0−5.5	4.16
[BPh]dA6(H2)−dG18(NH1)	2.8−3.2	2.73
Exchangeable Protons (Carcinogen−DNA)		
[BPh]dA6(NH6)−BPh(H2)	2.2−4.0	2.89
[BPh]dA6(NH6)−BPh(H3)	2.2−4.0	2.73
dG16(NH1)−BPh(H9)	3.5−5.0	4.34
dT17(NH3)−BPh(H2)	3.0−5.5	5.77
dT17(NH3)−BPh(H3)	3.0−5.5	5.61
Nonexchangeable Protons (DNA−DNA)		
[BPh]dA6(H8)−dC5(H1′)	>5.3	5.40
[BPh]dA6(H8)−[BPh]dA6(H3′)	2.5−4.5	4.42
[BPh]dA6(H8)−dC7(H5)	2.7−4.0	3.12
Nonexchangeable Protons (Carcinogen−DNA)		
[BPh]dA6(H1′)−BPh(H11)	4.7−6.0	4.45
[BPh]dA6(H2)−BPh(H9)	4.5−6.0	5.44
[BPh]dA6(H2)−BPh(H10)	4.5−6.0	4.66
[BPh]dA6(H8)−BPh(H11)	4.7−6.0	5.18
dG16(H1′)−BPh(H7)	2.8−4.0	3.74
dG16(H1′)−BPh(H8)	3.5−5.5	3.21
dG16(H1′)−BPh(H9)	4.7−6.0	4.66
dG16(H2′)−BPh(H7)	2.0−3.7	2.52
dG16(H2′)−BPh(H8)	3.8−5.5	3.86
dG16(H3′)−BPh(H7)	4.6−6.0	4.86
dG16(H3′)−BPh(H8)	4.7−6.0	5.44
dG16(H8)−BPh(H6)	3.4−4.5	3.36
dG16(H8)−BPh(H7)	3.4−4.5	3.22
dG16(H8)−BPh(H8)	4.7−6.0	4.81
dT17(H1′)−BPh(H8)	4.3−5.7	3.89
dT17(H1′)−BPh(H9)	3.5−5.7	3.21
dT17(CH_3)−BPh(H5)	4.0−6.0	4.50
dT17(CH_3)−BPh(H6)	2.7−3.5	2.80
dT17(CH_3)−BPh(H7)	2.8−3.5	2.47
dT17(CH_3)−BPh(H8)	3.2−5.1	4.00
dT17(H6)−BPh(H7)	3.5−5.5	3.39
dT17(H6)−BPh(H8)	3.2−4.1	3.10

All of the BPh−DNA exchangeable and nonexchangeable proton distance restraints involve NOEs between the benzo[*c*]phenanthrenyl protons of the carcinogen and the [BPh]dA6•dT17 and dC7•dG16 base pairs of the nucleic acid (Table 2; numbered cross peaks, Figures 2B, S1 (supplementary material), 3 and 5). The combined pattern of these specific carcinogen−DNA NOEs (Table 2) and upfield chemical shifts (Table S3 (supplementary material), Figure 4) presented earlier unambiguously establishes that the benzo[*c*]phenanthrenyl ring, which is covalently linked at the N^6 of dA6, is intercalated 3′ to the lesion site between the [BPh]dA6•dT17 and dC7•dG16 base pairs in the (−)-*trans-anti*-[BPh]dA•dT 11-mer duplex.

Phosphorus Spectra. The proton-decoupled phosphorus spectrum of the (−)-*trans-anti*-[BPh]dA•dT 11-mer duplex exhibits two downfield-shifted phosphorus resonances that

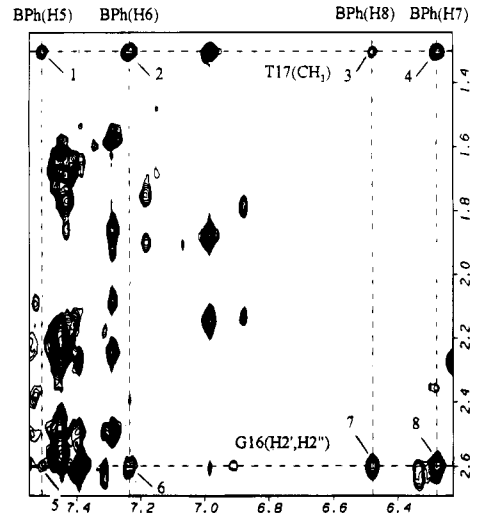

FIGURE 5: Expanded NOESY (300 ms mixing time) contour plot of the (−)-*trans-anti*-[BPh]dA•dT 11-mer duplex in D_2O buffer at 25 °C. The cross peaks 1−8 identify carcinogen−DNA NOEs between the benzo[*c*]phenanthrenyl protons and the DNA protons and are assigned as follows: 1, BPh(H5)−T17(CH_3); 2, BPh(H6)−T17(CH_3); 3, BPh(H8)−T17(CH_3); 4, BPh(H7)−T17(CH_3); 5, BPh(H5)−G16(H2′/H2″); 6, BPh(H6)−G16(H2′/H2″); 7, BPh(H8)−G16(H2′/H2″); 8, BPh(H7)−G16(H2′/H2″).

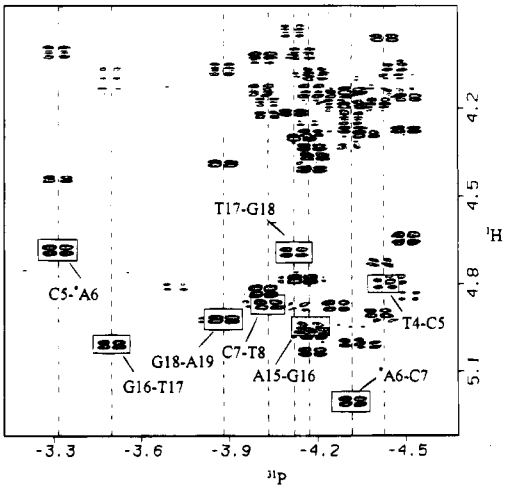

FIGURE 6: Contour plot of the proton-detected phosphorus−proton heteronuclear correlation experiment on the (−)-*trans-anti*-[BPh]-dA•dT 11-mer duplex in D_2O buffer at 25 °C. The phosphorus assignments for (n)-^{31}P-(n + 1) steps in the central d(T4-C5-[BPh]-A6-C7-T8)•d(A15-G16-T17-G18-A19) segment are listed as follows: dT4-dC5, −4.42 ppm; dC5-[BPh]dA6, −3.31 ppm; [BPh]-dA6-dC7, −4.32 ppm; and dC7-dT8, −4.03 ppm on the modified strand and dA15-dG16, −4.18 ppm; dG16-dT17, −3.49 ppm; dT17-dG18, −4.12 ppm; and dG18-dA19, −3.87 ppm on the unmodified strand. The correlation cross peaks between the phosphorus and its 5′-linked sugar H3′ protons are boxed for this central segment.

are outside the typical unperturbed −4.0 to −4.5 ppm B-DNA region. The phosphorus spectrum has been assigned from an analysis of an indirect detection, proton−phosphorus heteronuclear correlation experiment (Figure 6). Each non-terminal phosphorus can be correlated with its 5′-linked H3′ proton (three-bond H−P coupling) and its 3′-linked H4′ proton (four-bond H−P coupling) in the two-dimensional plot (Figure 6), and the phosphorus resonances can be assigned on the basis of the known H3′ and H4′ sugar proton assignments. The most downfield-shifted phosphorus resonance (−3.31 ppm) is assigned to the dC5-[BPh]dA6 step, while the next most downfield-shifted phosphorus resonance (−3.49 ppm) is assigned to the dG16-dT17 step in the (−)-*trans-anti*-[BPh]dA•dT 11-mer duplex (Figure 6).

Molecular Mechanics Computations. The search strategy employed began with a B-DNA (Arnott et al., 1976) central three base pair d(C5-[BPh]A6-C7)•d(G16-T17-G18) segment of the (−)-*trans-anti*-[BPh]dA•dT 11-mer duplex. The BPh−DNA orientation space was searched with 16 energy minimization trials, in which α′ ([BPh]dA6(N^1)−[BPh]dA6-(C^6)−[BPh]dA6(N^6)−BPh(C^1)) and β′([BPh]dA6(C^6)−[BPh]-dA6(N^6)−BPh(C^1)−BPh(C^2)) were each started at 0°, 90°, 180°, and 270° in all combinations, and the DNA starting conformation was the energy-minimized B form. Searching orientation space at 90° intervals of α′ and β′ is an excellent procedure for locating all the important potential energy wells, because our minimization protocol permits torsion angle variations of up to 100° in each minimization step (Hingerty et al., 1989). Consequently, energy minima in each quadrant of α′ and β′ are accessible, and the reduced variable domain of torsion angle space greatly enhances the likelihood of finding the important structures. In these trials, the DUPLEX hydrogen bond penalty function (Hingery et al., 1989) for Watson−Crick base pairing was utilized at all base pairs, since the NMR data indicated that the modified base pair was hydrogen bonded, and NMR-derived upper and lower bound distance restraints listed in Table 2 were included.

Of the sixteen structures of the d(C5-[BPh]A6-C7)•d(G16-T17-G18) segment computed, four were identified as being in the family of structures in which the benzo[*c*]phenanthrenyl ring of the (−)-*trans-anti*-[BPh]dA6 adduct intercalates in the 3′-direction and is sandwiched between intact Watson−Crick [BPh]dA6•dT17 and dC7•dG16 base pairs. The pairwise RMS deviation of these four trimers ranges between 0.77 and 1.44 Å. Two views showing the superposition of these four structures, which also exhibited the best fit to the NMR data as indicated by their corresponding goodness-of-fit values of F_N and F_{NN} for eqs 1 and 2, respectively, with W = 15 kcal/mol•Å^2 (Materials and Methods section), are plotted in Figure 7. The corresponding F_N, F_{NN}, and energy values of these four trimers are summarized in the caption of Figure 7, and the distributions of their sugar pseudorotation (P) and glycosidic (χ) torsion angles for the central trimer residues are given in Table S4 of the supplementary material. We chose to embed the conformer (structure **4**) with the best goodness-of-fit values (F_N = 0.0 and F_{NN} = 2.3) into an energy-minimized B-form 11-mer corresponding to the sequence of the adduct duplex **2**. This 11-mer was reminimized with all restraints. Subsequently, the hydrogen bond penalty function and the distance restraints were released with energy minimization in one step, yielding a final unrestrained structure for the (−)-*trans-anti*-[BPh]dA•dT 11-mer duplex that has low energy (−568 kcal/mol) and fits the NMR-derived distance restraints (Table 2).

Solution Structure. A view normal to the helix axis and looking into the major groove of the central d(C5-[BPh]A6-C7)•d(G16-T17-G18) segment of the NMR energy-minimized structure of the (−)-*trans-anti*-[BPh]dA•dT 11-mer duplex is shown in Figure 8A. The covalently linked benzo-[*c*]phenanthrenyl ring intercalates to the 3′-side of the modification site without disruption of the Watson−Crick hydrogen-bonding alignment of the modified [BPh]dA6•dT17 or flanking dC5•dG18 and dC7•dG16 base pairs. An intercalation pocket between the [BPh]dA6•dT17 and

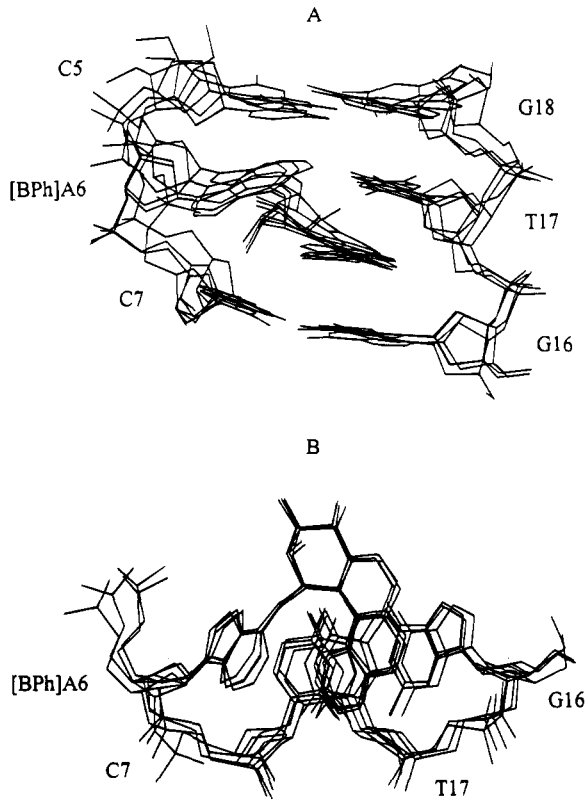

FIGURE 7: Superposition of the four trinucleotide segments that best fit the NMR data of the (−)-*trans-anti*-[BPh]dA6 adduct obtained from the 16 trials to search conformational space using NMR restraints (Table 2) and the program DUPLEX. (A) View looking into the major groove of the central d(C5-[BPh]A6-C7)•d(G16-T17-G18) trinucleotide segment and (B) view looking down the helix axis of the d([BPh]A6-C7)•d(G16-T17) segment. The relative goodness-of-fit to the NMR data was determined by evaluating eqs 1 and 2 (Materials and Methods section) for F_N and F_{NN}, which indicate the magnitude of the deviation of the distances in the model from the given upper and lower bounds, respectively, of the corresponding distance restraints. The energy, F_N, and F_{NN} values (in kcal/mol) of these four structures are as follows: structure **1**, $E = -105.5$, $F_N = 0.1$, $F_{NN} = 6.3$; structure **2**, $E = -90.9$, $F_N = 2.1$, $F_{NN} = 1.6$; structure **3**, $E = -120.9$, $F_N = 0.4$, $F_{NN} = 3.2$; structure **4**, $E = -115.9$, $F_N = 0.0$, $F_{NN} = 2.3$.

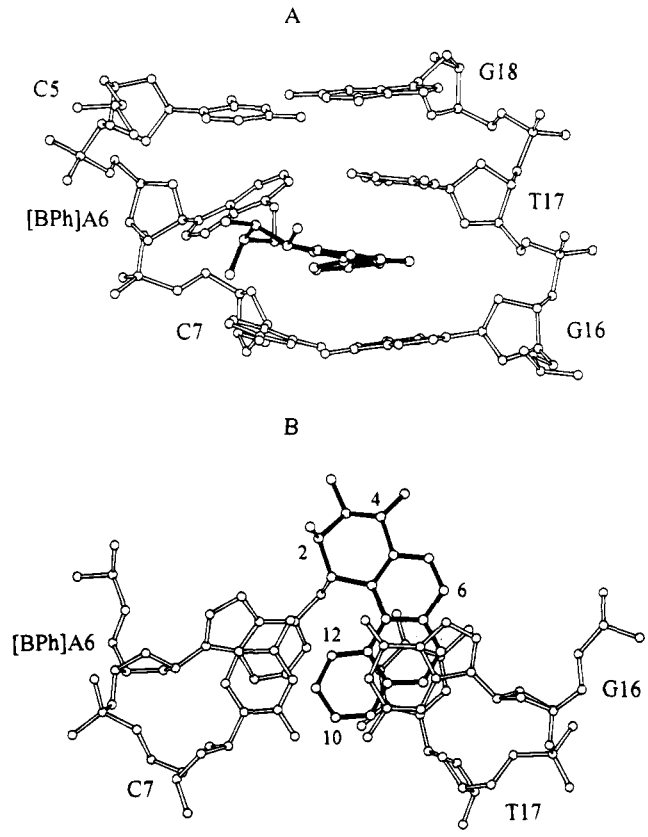

FIGURE 8: (A) View looking into the major groove and normal to the helix axis of the central d(C5-[BPh]A6-C7)•d(G16-T17-G18) segment of the NMR energy-minimized structure of the (−)-*trans-anti*-[BPh]dA•dT 11-mer duplex. The BPh ring system is shown in darkened bonds and is intercalated between the d([BPh]A6-C7)•d(G16-T17) base pairs. (B) View looking down the helix axis for the d([BPh]A6-C7)•d(G16-T17) segment of the (−)-*trans-anti*-[BPh]-dA•dT 11-mer duplex. The benzylic ring resides in the major groove, while the phenanthrenyl ring of [BPh]dA6 overlaps predominantly with the dG16 and dT17 residues. These drawings were prepared using Molscript V1.1 (Kraulis, 1991).

dC7•dG16 base pairs for the phenanthrenyl ring system is generated by doubling the distance between the dG16 and dT17 residues on the unmodified strand, as measured by the distance (6.71 Å) between the dG16(NH1) and dT17(NH3) imino protons. A view of the entire 11-mer adduct duplex is shown in Figure S2 of the supplementary material.

Quantitative analyses of the rise distances and twist angles between pairs of residues proceeding from the 5′- to the 3′-direction along each strand, and of the degree of buckle and propeller twist of each base pair in the entire adduct duplex, are plotted in Figure S3 of the supplementary material [computed using the approach of Babcock et al. (1993)]. The [BPh]dA6•dT17 pair is propeller twisted by −22.7° (Figure S3D (supplementary material)) and buckled by 32.1° (Figure S3C) (supplementary material)), with the major groove edges of [BPh]dA6 and of the flanking 3′-side dC7 residue positioned close together in space (Table 2). This orientation results in a wedge-shaped intercalation site at the [BPh]dA6-dC7 step on the modified strand (rise = 5.6 Å, Figure S3B (supplementary material)), while the dG16 and dT17 bases at the dG16-dT17 step on the unmodified strand remain far apart (rise = 6.5 Å, Figure S3B (supplementary material)) and approximately parallel to each other (Figures S3 (supplementary material) and 8A).

A view looking down the helix axis of the central two base pair d([BPh]A6-C7)•d(G16-T17) segment of the NMR−molecular mechanics structure of the (−)-*trans-anti*-[BPh]-dA•dT 11-mer duplex (Figure 8B) emphasizes the overlap geometry between the phenanthrenyl ring system and the dG16 and dT17 bases on the unmodified strand. This alignment positions the nonplanar benzylic ring of BPh in the major groove, with the phenanthrenyl ring inserting into the intercalation site and projecting toward the minor groove edge of the helix. The benzylic ring adopts a distorted half-chair conformation with the BPh(H1) and BPh(H2) protons in pseudo-diequatorial orientations, while the BPh(H3) and BPh(H4) protons are in pseudo-diaxial orientations. The potential steric clash between the benzylic BPh(H1) and phenanthrenyl BPh(H12) protons in the fjord region of the BPh molecule is relieved by a propeller-like distortion of the aromatic phenanthrenyl ring away from planarity (Figure 8A), which is defined by the −15.8° value obtained for the $C^{4B}-C^{6B}-C^{8B}-C^{12}$ dihedral angle.

The carcinogen−base linkage site for the [BPh]dA6 residue is defined by the angles α′ ([BPh]dA6(N^1)−[BPh]-dA6(C^6)−[BPh]dA6(N^6)−BPh(C^1) = 229°) and β′ ([BPh]-dA6(C^6)−[BPh]dA6(N^6)−BPh(C^1)−BPh(C^2) = 249°) in the

NMR−molecular mechanics structure of the (−)-*trans-anti*-[BPh]dA•dT 11-mer duplex. The glycosidic torsion angles, sugar puckers, and backbone torsion angles for the d(C5-[BPh]A6-C7)•d(G16-T17-G18) segment of the (−)-*trans-anti*-[BPh]dA•dT 11-mer duplex are listed in Table S5 of the supplementary material. The sugar pucker pseudorotation parameters (Altona & Sundaralingham, 1972) of residues dC7 (O1′-*exo*), dG16 (O1′-*exo*), and dT17 (O4′-*endo*) that flank the intercalation site deviate from the C2′-*endo* domain, but remain within the range of sugar pucker conformations found in B-DNA crystals. The glycosidic torsion angle at the [BPh]dA6 modification site adopts a high *anti* conformation with $\chi = 294°$ (Table S5 (supplementary material)). All remaining backbone torsion angles and sugar pseudorotation parameters in the adduct duplex fall within or near the B_1-DNA conformation.

Convergence to very similar final structures resulted when the NMR−molecular mechanics structure was distorted by +45° or −45° at each of the two bonds (α′ and β′) at the base−carcinogen linkage and reminimized with restraints. Two views of the best fit superposition of the resulting four structures are plotted in Figure S4 of the supplementary material.

DISCUSSION

Spectral Quality. Despite the presence of minor peaks, well-resolved imino (Figure 1A) and nonexchangeable proton resonances (Figure 1B) are observed for the (−)-*trans-anti*-[BPh]dA•dT 11 mer duplex. The NOE connectivities involving exchangeable protons (Figure 2) and nonexchangeable protons (Figure 3) can be readily followed in the NOESY data sets, thus permitting the assignment of nucleic acid (Table 1) and carcinogen (Figure 4) protons in the adduct duplex. Cross peaks originating from one or more minor species of unknown identity are also observed in the NOESY spectra, but fortunately do not overlap significantly with cross peaks pertaining to the major conformation of the (−)-*trans-anti*-[BPh]dA•dT 11-mer duplex. In addition, a series of well-resolved carcinogen−DNA NOEs between the benzo[*c*]phenanthrenyl and nucleic acid protons (numbered cross peaks in Figures S1 (supplementary material), 2B, 3 and 5) is also observed and provides the restraints (Table 2) necessary for alignment of the carcinogen along the helix.

Base Pairing at the Intercalation Site. The intercalation site for the covalently attached benzo[*c*]phenanthrenyl ring system is generated without disruption of the Watson−Crick alignments of the [BPh]dA6•dT17 and dC7•dG16 base pairs that flank it (Figure 8A). However, the [BPh]dA6•dT17 base pair is propeller twisted such that the adjacent dC5•dG18 base pair is closer to the minor groove edge than to the major groove edge of [BPh]dA6 (Figure 8A). This propeller twist orientation of the modified base pair is supported by the observation of a stronger NOE from the imino proton of dG18 to the minor groove [BPh]dA6(H2) proton (peak F, Figure 2B) relative to the major groove [BPh]dA6(NH6) proton (peak E, Figure 2B). In addition, the major groove [BPh]dA6(H8) proton exhibits an NOE to the major groove C7(H5) proton (peak a, Figure 3) in the [BPh]dA6-dC7 step, but not to the minor groove C5(H1′) proton (box b, Figure 3) in the C5-[BPh]dA6 step. These combined experimental results establish the orientation of the propeller twist of the modified [BPh]dA6•dT17 base pair relative to the flanking dC5•dG18 and dC7•dG16 base pairs. The NH6 amino proton of [BPh]dA6 at the linkage site is rotated out of the plane of the adenine ring ([BPh]dA6(C^6)−[BPh]dA6(N^6)−[BPh]dA6(NH^6) angle = 110°), allowing the [BPh]dA6(N^6)−BPh(C^1) bond to orient in a way that facilitates the intercalation of the carcinogen into the helix.

Intercalation Site Geometry and Stacking Interactions. The intercalation site is buckled in the NMR−molecular mechanics structure of the adduct duplex (Figure 8A) such that dG16 and dT17 are approximately parallel to each other (and hence their protons are further apart, rise = 6.5 Å, Figure S3B (supplementary material)), while [BPh]dA6 and dC7 are wedge shaped (and hence their protons are close to each other, rise = 5.6 Å, Figure S3B (supplementary material)). This greater separation at the dG16-dT17 step is a consequence of the phenanthrenyl ring being sandwiched predominantly between the dG16 and dT17 bases on the unmodified strand (Figure 8A). This buckled geometry for the intercalation site is supported experimentally by the absence of an NOE between the dG16(H1′) and dT17(H6) protons for the dG16-dT17 step on the unmodified strand (box c, Figure 3), in contrast to the presence of an NOE between the [BPh]dA6(H1′) and dC7(H6) protons for the [BPh]dA6-dC7 step on the modified strand (Figure 3).

The sugar pucker conformations of dT17 (O4′-*endo*) and of dC7 and dG16 (C1′-*exo*) (Table S5 (supplementary material)) contrasts to that of [BPh]dA6 (C2′-*endo*), all of which are located at the intercalation site. The glycosidic torsion angle χ for [BPh]dA6 (294°) is high *anti*. All remaining sugar puckers, glycosidic bonds, and backbone torsion angle values are in or very close to the representative parameters prevalently observed for B-DNA (Table S5 (supplementary material)).

There is a shearing of the base pairs flanking the intercalation site, with dG16 and dT17 on the unmodified strand stacked more directly over each other and over the intercalated phenanthrenyl ring system (Figure 8B). The dramatic >1.5 ppm upfield shifts observed for the imino protons of dG16 and dT17 (Figure 1A and Table S3 (supplementary material)) and for several aromatic phenanthrenyl ring protons (Figure 4) provide experimental support for intercalation of the phenanthrenyl ring. By contrast, [BPh]dA6 and dC7 on the modified strand do not stack with the intercalated phenanthrenyl ring (Figure 8B). The loss of stacking interactions between the modified adenine and dC7 explains why moderate downfield chemical shifts are observed for the major groove base and sugar protons of dC7 in the adduct duplex relative to the control duplex (Figure 8B, Table S3 (supplementary material)). The moderate upfield shifts of the minor groove sugar protons of dC5 in the adduct duplex (Table S3 supplementary material)) can also be explained by the propeller twist and buckling of the modified base pair, which align the minor groove edge of the aromatic purine ring of [BPh]dA6 closer to dC5 (Figure 8A).

Unperturbed aromatic phenanthrenyl ring protons have chemical shift values in the 8.0−8.5 ppm range, but they experience distinct upfield shifts upon adduct formation (Figure 4) that are dependent upon the stacking geometry between the phenanthrenyl ring and the flanking base pairs at the intercalation site. Thus, the BPh(H5) and BPh(H6) protons experience small upfield shifts of ~0.5 ppm since

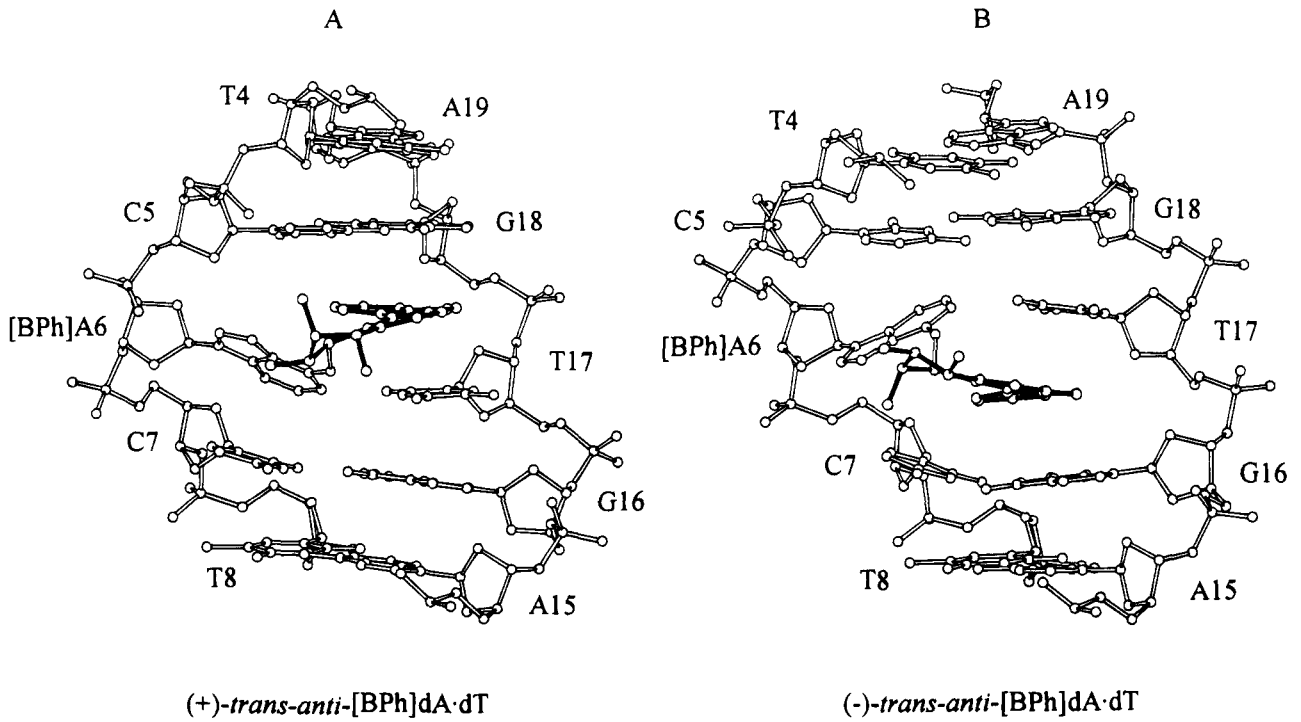

FIGURE 9: View looking into the major groove and normal to the helix axis of the solution structure of the central d(T4-C5-[BPh]A6-C7-T8)·d(A15-G16-T17-G18-A19) segment of (A) the (+)-*trans-anti*-[BPh]dA·dT 11-mer duplex and (B) the (−)-*trans-anti*-[BPh]dA·dT 11-mer duplex. The benzo[*c*]phenanthrenyl moiety, shown in darkened bonds, is intercalating in the 5′-side direction of the lesion site between d(C5-[BPh]A6)·d(T17-G18) base pairs in the (+)-*trans-anti* isomer (A) and in the 3′-side direction between d([BPh]A6-C7)·d(G16-T17) base pairs in the (−)-*trans-anti* isomer. Figures were prepared using Molscript V1.1 (Kraulis, 1991).

they are located the farthest from the DNA helix axis, in contrast to the BPh(H11) proton, which is shifted upfield by ~3 ppm and is located toward the center of the helix (Figure 8B). Two of the three aromatic rings of the phenanthrenyl chromophore stack directly over the dG16 and dT17 bases, thereby positioning their attached protons [extending from BPh(H7) to BPh(H10)] on the periphery of the flanking purine and pyrimidine bases (Figure 8B) and accounting for the observed moderate upfield shifts of these BPh protons.

The benzylic ring is located in the major groove, while the long axis of the phenanthrenyl ring system is positioned within the DNA helix, with two of its aromatic rings stacking directly with the flanking dG16 and dT17 bases on the complementary strand (Figure 8B). Thus, the BPh(H6), BPh(H7), and BPh(H8) protons, which lie along the outside edge of the phenanthrenyl ring, show NOEs exclusively to the base and sugar protons of dG16 and dT17 (Table 2). The BPh(H6) proton is located on the phenanthrenyl ring residing chiefly in the major groove (Figure 8B), and thus exhibits NOEs to the flanking major groove dG16(H8) and T17(CH_3) protons (Table 2). By contrast, the BPh(H9) proton is located on the phenanthrenyl ring directly facing the minor groove (Figure 8B) and thus exhibits NOEs to the minor groove sugar H1′ protons of both dG16 and dT17 (Table 2). The BPh(H7) and BPh(H8) protons reside on the phenanthrenyl ring that is sandwiched directly between dG16 and dT17 (Figure 8B), and they exhibit NOEs with both minor and major groove base and sugar protons of these flanking DNA bases (Table 2). We also observe NOEs between the BPh(H9), BPh(H10), and BPh(H11) protons, which are located on the phenanthrenyl ring closest to the center of the helix (Figure 8B), and the H8, H2, and H1′ protons of [BPh]dA6 (Table 2). Moreover, the exchangeable dT17 and dG16 imino and [BPh]dA6(NH6) amino protons each exhibit several NOEs to the benzylic and phenanthrenyl protons in the adduct duplex (Table 2, Figure 2B). These carcinogen−DNA NOEs independently establish that the phenanthrenyl ring intercalates between the [BPh]dA6·dT17 and dC7·dG16 base pairs and permit definitive alignment of the benzylic ring and the three intercalated aromatic phenanthrenyl rings with respect to the major and minor grooves of the (−)-*trans-anti*-[BPh]dA·dT 11-mer duplex.

Comparison of the Solution Structures of the (+)-trans-anti- and (−)-trans-anti-[BPh]dA·dT 11-mer Duplexes. It is of interest to compare the alignment of the (−)-*trans-anti*-[BPh]dA·dT 11-mer duplex reported in this paper with the corresponding alignment of the isomeric (+)-*trans-anti*-[BPh]dA·dT 11-mer duplex in the same sequence context reported previously from our laboratory (Cosman et al., 1993b). The thermal transition midpoints (t_m) at optical concentrations (~10 μM in strands) for the control duplex (t_m = 43.8 ± 0.5 °C) and for both the (+)- and (−)-*trans-anti*-[BPh]dA·dT 11-mer duplexes (t_m = 43.3 ± 0.5 °C for both adducts) have been measured by UV spectroscopic methods (Laryea et al., 1994). The similar t_m values for the control and for both stereoisomeric adduct duplexes indicate that their relative thermal stabilities are comparable to one another, thereby permitting us to undertake NMR studies (at millimolar concentrations) of these adduct-containing duplexes at ambient temperature.

Views looking normal to the helix axis and into the major groove of the central d(T4-C5-[BPh]A6-C7-T8)·d(A15-G16-T17-G18-A19) segment of the NMR−molecular mechanics structures of the isomeric (+)-*trans-anti*-[BPh]dA·dT 11-mer [Figure 9A, Cosman et al. (1993b)] and (−)-*trans-anti*-[BPh]-dA·dT 11-mer (Figure 9B, present work) duplexes show that the phenanthrenyl ring intercalates to the 5′-side of the

modified adenine in the (+)-*trans-anti* adduct, while it intercalates to the 3′-side in the (−)-*trans-anti* stereoisomer. In both cases, the modified [BPh]dA•dT and flanking dG•dC base pairs retain their Watson−Crick alignment, and the [BPh]dA•dT pair is propeller twisted and buckled with the amino protons of [BPh]dA6 of both adducts rotated out of the plane of the modified adenine to facilitate the insertion of the phenanthrenyl ring into the helix.

A comparison of the overlap geometry of the phenanthrenyl ring at the intercalation site of the d(C5-[BPh]A6)•d(T17-G18) segment of the (+)-*trans-anti*-[BPh]dA•dT 11-mer duplex (Figure S5A (supplementary material) to that of the d([BPh]A6-C7)•d(G16-T17) segment of the (−)-*trans-anti*-[BPh]dA•dT 11-mer duplex (Figure S5B (supplementary material)) addresses other similarities in the structures of both adducts, in that the nonplanar benzylic ring is located in the major groove of the modified helix with the aromatic phenanthrenyl ring inserted into the helix and stacking predominantly with the dT17 base and either the 5′-side dG18 [(+)-*trans-anti*] (Figure S5A (supplementary material)) or the 3′-side dG16 [(−)-*trans-anti*] (Figure S5B (supplementary material)) base. Interestingly, the chemical shifts of the phenanthrenyl protons in the (+)-*trans-anti*-[BPh]dA•dT 11-mer duplex have values similar to those found in the (−)-*trans-anti*-[BPh]dA•dT 11-mer duplex (Figure 4). The BPh(H11) aromatic proton is the most upfield shifted, while BPh(H5) exhibits the smallest upfield shift in both adduct duplexes.

The difference in the 5′- and 3′-directions of the intercalation site reflects the chiral nature of the precursor (+)- and (−)-*anti*-BPhDE enantiomers and their reaction with adenine to form (+)- and (−)-*trans-anti*-[BPh]dA adducts. Although both the (+)- and (−)-*trans-anti*-[BPh]dA•dT 11-mer duplex adducts have several features in common, as outlined earlier, there are subtle differences in the structures of each adduct that reflect the chirality of DNA and the asymmetric orientation of the 5′ and 3′ intercalation sites along the right-handed DNA helix. The benzylic ring of the (+)-*trans-anti*-[BPh]dA stereoisomer (Figure S5A (supplementary material)) stacks over the major groove edge of the flanking dC5 base, in contrast to the benzylic ring of the (−)-*trans-anti*-[BPh]-dA isomer (Figure S5B (supplementary material)), which is completely isolated and does not overlap with any of the flanking DNA residues.

Two other striking differences between the stereoisomeric (+)- and (−)-*trans-anti*-[BPh]dA•dT 11-mer duplexes are observed that involve the benzylic ring pucker conformation and the direction of the propeller-like distortion of the aromatic phenanthrenyl ring, and these differences, in turn, also contribute to the asymmetrical orientation of the 5′ and 3′ intercalation sites along the DNA helix. It has previously been reported that the deoxyribonucleoside *trans* adducts, derived from (+)- and (−)-*anti*-BPhDE (Agarwal et al., 1987) and other bay region polycyclic aromatic hydrocarbon diol epoxides derived from either benzo[*a*]pyrene (Cheng et al., 1989) or 5-methylchrysene (Reardon et al., 1989), adopt half-chair conformations in which the two benzylic protons farthest away from the binding site [BPh(H3) and BPh(H4) in the present work] are in pseudo-diaxial orientations. Our previous work on benzo[*a*]pyrene diol epoxide-modified dG *trans* adducts in oligodeoxyribonucleotide duplexes (Cosman et al., 1992; De los Santos et al., 1992), as well as the present work on the (−)-*trans-anti*-[BPh]dA•dT 11-mer duplex, shows agreement with this orientation for these two protons upon proceeding from the nucleoside adduct to the oligomer duplex level. By contrast, our previous work on the (+)-*trans-anti*-[BPh]dA•dT 11-mer duplex (Cosman et al., 1993b) showed that the orientation of the BPh(H3) and BPh(H4) protons is pseudo-diequatorial, which differs from all the other PAH−DNA *trans* oligomeric duplex adducts and their nucleoside analog adducts studied to date. In addition, the benzylic BPh(H1) and BPh(H2) protons are oriented in a pseudo-diaxial position in the (+)-*trans-anti*-[BPh]dA•dT 11-mer duplex (Cosman et al., 1993b), in contrast to the pseudo-diequatorial orientation found in the stereoisomeric (−)-*trans-anti*-[BPh]dA•dT 11-mer duplex (present work). This difference in the orientation of the benzylic protons of the (+)- and (−)-*trans-anti*-[BPh]dA-modified duplexes indicates that the conformation of the benzylic ring adjusts to fit the circumstances of its surrounding environment. While BPh(H3) and BPh(H4) are pseudo-diaxial in most *trans* PAH−DNA nucleotide and duplex adducts, intercalation of the covalently attached BPh to the 5′-side of the lesion site in a duplex may be facilitated or stabilized when these protons are in a pseudo-diequatorial orientation.

The direction of the propeller-like distortion of the phenanthrenyl ring that relieves the strain in the sterically hindered fjord region of BPh defined by the dihedral angle $C^{4B}-C^{6B}-C^{8B}-C^{12}$ is +18.1° in the (+)-*trans-anti*-[BPh]-dA adduct (Figure 9A) and −15.8° in the (−)-*trans-anti*-[BPh]dA adduct (Figure 9B). In both cases, the direction of the distortion optimizes the stacking interactions between the phenanthrenyl ring and the flanking guanine purine ring, which is either the 5′-side dG18 base in the (+)-*trans-anti* adduct or the 3′-side dG16 base in the (−)-*trans-anti* adduct.

Summary. Our previous and ongoing NMR computational studies on the structures of stereoisomeric polycyclic aromatic hydrocarbon (PAH)−DNA adducts to date have provided us not only with structural details at the molecular level of the PAH−DNA alignments but also with valuable insights with regard to the effects of chirality on adduct orientations relative to the 5′- and 3′-DNA strand polarity. Such stereochemically defined 5′ and 3′ orientational differences in adduct conformations involving chiral pairs of PAH diol epoxide enantiomer precursors may be a general feature of covalent adduct formation. In turn, these structural differences may have profound effects on the function of a variety of enzymes and thus account for the differences in the biological effects induced by mirror-image PAH diol epoxide stereoisomers. As a result of the availability of site specific and stereochemically defined adducts derived from the covalent reactions of PAH diol epoxides with DNA, significant new information along these lines is beginning to emerge.

We have shown here and elsewhere (Cosman et al., 1993b) that the intercalated phenanthrenyl residues covalently attached to the major groove N^6-position of adenine are situated on the 5′-side and 3′-side of the modified bases in adducts derived from (+)-BPhDE and (−)-BPhDE, respectively, without disruption of the modified [BPh]dA•dT and flanking dG•dC base pairs. These structural studies have shown that although these isomeric (+)- and (−)-*trans-anti*-[BPh]dA adducts have several similarities in common they differ from one another not only in the orientation relative to 5′- and 3′-strand polarity but also in the benzylic ring pucker

conformation and orientation of the propeller-like distortion.

Interestingly, differences in the 5′- and 3′-directionality along the helical axis of covalently attached bulky polycyclic aromatic hydrocarbons are also observed in the *trans* addition products derived from the binding of the enantiomeric (+)- and (−)-*anti*-BPDEs to the minor groove N^2-position of dG in duplex DNA. In these adducts, the benzo[*a*]pyrenyl aromatic ring resides in the minor groove of a minimally perturbed DNA duplex and is directed toward the 5′-end of the modified strand in the (+)-*trans-anti*-[BP]dG adduct (Cosman et al., 1992) or toward the 3′-end in the (−)-*trans-anti*-[BP]dG adduct (De los Santos et al., 1992). These directional orientations relative to the modified guanosyl residues are maintained even in single-stranded DNA and give rise to susceptibilities to enzymatic by the exonucleases phosphodiesterase I and II (Mao et al., 1993), which digest DNA progressively from the 3′-end and from the 5′-end, respectively. Analogous effects have been observed with the (+)- and (−)-*trans-anti*-[BPh]dA adducts at the duplex level from structural studies (this work), as well as at the strand level from enzymatic digestion studies (Laryea et al., manuscript in preparation).

The results of a few other investigations on the biochemical consequences of stereochemically isomeric adducts derived from the binding of enantiomeric PAH diol epoxides to DNA have been published. When DNA synthesis is catalyzed by Pol I (Klenow fragment, exonuclease-free) *in vitro*, nucleotide insertion opposite the base flanking the BP-N^2-dG lesion on the 5′-side is significantly more inhibited in the case of the (+)-*trans-anti* adduct than the (−)-*trans-anti* adduct (Shibutani et al., 1993). These observations are also consistent with the positioning of the pyrenyl ring toward the 5′-end of the modified strand in the (+)-*trans-anti*-[BP]-dG·dC 11-mer duplex (Cosman et al., 1992) and modified (+)-*trans-anti*-[BP]dG single-stranded deoxyribooligonucleotides (Mao et al., 1993). However, adduct conformations at replication forks may well be different from those found in double-stranded and single-stranded DNA, because the complementary primer strand extends up to the lesion on the template strand only. The structural features of such replication forks are currently under investigation in our laboratory. Other studies with site specific (+)- and (−)-*anti*-BP-N^2-dG adducts show that they can inhibit the elongation of transcripts catalyzed by T7 RNA polymerase to different extents, depending on the stereochemical properties of the adducts (Choi et al., 1994). Finally, it has been shown that polyclonal and monoclonal antibodies developed against DNA modified by racemic *anti*-BPDE exhibit differences in selectivity toward (+)- and (−)-*trans-anti*-[BP]-dG adducts (Venkatachalam & Wani, 1994) embedded in the same sequence context as those studied earlier by NMR (Cosman et al., 1992; De los Santos et al., 1992). The polyclonal antibody preferentially recognizes the (+)-*trans-anti*-[BP]dG adduct derived from the highly tumorigenic (+)-*anti*-BPDE, while the monoclonal antibody binds much more strongly to the nontumorigenic (−)-*trans-anti*-[BP]dG adduct (Venkatachalam & Wani, 1994). This apparent preference of difference antibodies for distinct stereoisomeric (+)- and (−)-*trans-anti*-[BP]dG adducts may in part be due to the striking differences in the 5′- and 3′-orientation of the pyrenyl ring along the helix in the solution structures of these adducts.

The availability of site specific and stereochemically defined [BPh]dA adducts is likely to lead to new studies, which will enhance our understanding of the relationships between their structural characteristics and their biological effects and activities.

ACKNOWLEDGMENT

We thank Professor Wilma K. Olson (Chemistry Department, Rutgers University) for sharing with us unpublished analyses of pseudorotation parameters in B-DNA crystal structures deposited in the Nucleic Acids Data Bank.

SUPPLEMENTARY MATERIAL AVAILABLE

Five tables listing exchangeable and nonexchangeable proton chemical shifts for the entire adduct duplex, proton chemical shift differences on adduct formation, distribution of P and χ torsion angles for the four calculated trimer segments, and backbone torsion angles of the NMR energy-minimized structure for the central trinucleotide segment and five figures showing an expanded NOESY contour plot in H_2O buffer, the NMR energy-minimized structure of the entire adduct duplex, the helical parameters (twist, rise, buckle, propeller twist) for the entire adduct duplex, the superposition of four structures derived following energy minimization with restraints from the NMR energy-minimized structure in which the α' and β' angles were changed by $\pm 45°$, and overlap geometries at the intercalation sites for the structures of the (+)-*trans-anti*- and (−)-*trans-anti*-[BPh]dA adducts opposite dT (15 pages). Ordering information is given on any current masthead page.

REFERENCES

Agarwal, S. K., Sayer, J. M., Yeh, H. J. C., Pannell, L. K., Hilton, B. D., Pigott, M. A., Dipple, A., Yagi, H., & Jerina, D. M. (1987) *J. Am. Chem. Soc. 109*, 2497−2504.

Altona, C., & Sundaralingam, M. (1972) *J. Am. Chem. Soc. 94*, 8205−8212.

Arnott, S., Bond, P. J., Seising, E., & Smith, P. J. (1976) *Nucleic Acids Res. 2*, 2459−2470.

Babcock, M. S., Pednault, E. P. D., & Olson, W. K. (1993) *J. Biomol. Struct. Dyn. 11*, 597−628.

Bigger, C. A. H., Strandberg, J., Yagi, H., Jerina, D. M., & Dipple, A. (1989) *Proc. Natl. Acad. Sci. U.S.A. 86*, 2291−2295.

Canella, K. A., Peltonen, K., Yagi, H., Jerina, D. M., & Dipple, A. (1992) *Chem. Res. Toxicol. 5*, 685−690.

Cheng, S. C., Hilton, B. D., Roman, J. M., & Dipple, A. (1989) *Chem. Res. Toxicol. 2*, 334−338.

Choi, D.-J., Marino-Alessandri, D. J., Geacintov, N. E., & Scicchitano, D. A. (1994) *Biochemistry 33*, 780−787.

Conney, A. H. (1982) *Cancer Res. 42*, 4875−4917.

Cosman, M., Ibanez, V., Geacintov, N. E., & Harvey, R. G. (1990) *Carcinogenesis 11*, 1667−1672.

Cosman, M., de los Santos, C., Fiala, R., Hingerty, B. E.. Singh, S., Ibanez, V., Margulis, L., Live, D., Geacintov, N. E., Broyde, S., & Patel, D. J. (1992) *Proc. Natl. Acad. Sci. U.S.A. 89*, 1914−1918.

Cosman, M., de los Santos, C., Fiala, R., Hingerty, B. E., Ibanez, V., Luna, E., Harvey, R., Geacintov, N. E., Broyde, S., & Patel, D. J. (1993a) *Biochemistry 32*, 4145−4155.

Cosman, M., Fiala, R., Hingerty, B. E., Laryea, A., Lee, H., Harvey, R., Amin, S., Geacintov, N. E., Broyde, S., & Patel, D. J. (1993b) *Biochemistry 32*, 12488−12497.

Cosman, M., Fiala, R., Hingerty, B. E., Amin, S., Geacintov, N. E., Broyde, S., & Patel, D. J. (1994a) *Biochemistry 33*, 11507−11517.

Cosman, M., Fiala, R., Hingerty, B. E., Amin, S., Geacintov, N. E., Broyde, S., & Patel, D. J. (1994b) *Biochemistry 33*, 11518−11527.

De los Santos, C., Cosman, M., Hingerty, B. E., Ibanez, V., Margulis, L., Geacintov, N. E., Broyde, S., & Patel, D. J. (1992) *Biochemistry 31*, 5245−5252.
Dipple, A., Pigott, M. A., Agarwal, S. K., Yagi, H., Sayer, J. M., & Jerina, D. M. (1987) *Nature 327*, 535−536.
Grimmer, G. (1993) *Polycyclic Arom. Compd. (Suppl.) 3*, 31−41.
Hare, D. R., Wemmer, D. E., Chou, S. H., Drobny, G., & Reid, B. R. (1983) *J. Mol. Biol. 171*, 319−336.
Harris, C. C. (1991) *Cancer Res. (Suppl.) 51*, 5023s−5044s.
Harvey, R. G. (1991) *Polycyclic Aromatic Compounds: Chemistry and Carcinogenicity*, Cambridge University Press, New York.
Hecht, S. S., El-Bayoumi, K., Rivenson, A., & Amin, S. (1994) *Cancer Res. 54*, 21−24.
Hingerty, B. E., Figueroa, S., Hayden, T., & Broyde, S. (1989) *Biopolymers 28*, 1195−1222.
Jerina, D. M., Yagi, H., Thakker, D. R., Sayer, J. M., van Bladeren, P. J., Lehr, R. E., Whalen, D. L., Levin, W., Chang, R. L., Wood, A. W., & Conney, A. H. (1984) in *Foreign Compound Metabolism* (Caldwell, J., & Paulson, G. D., Eds.) pp 13−32, Taylor & Francis, London.
Kraulis, P. J. (1991) *J. Appl. Crystallogr. 24*, 946−950.
Levin, W., Wood, A. W., Chang, R. L., Ittah, Y., Croisy-Delcey, M., Yagi, H., Jerina, D. M., & Conney, A. H. (1980) *Cancer Res. 40*, 3910−3914.
Levin, W., Chang, R. L., Wood, A. W., Ittah, Y., Thakker, D. R., Yagi, H., Jerina, D. M., & Conney, A. H. (1986) *Cancer Res. 46*, 2257−2261.
Lunde, G., & Bjorseth, A. (1977) *Nature 268*, 518−519.
Majumdar, A., & Hosur, R. V. (1992) *Prog. NMR Spectrosc. 24*, 109−158.
Mao, B., Li, B., Amin, S., Cosman, M., & Geacintov, N. E. (1993) *Biochemistry 32*, 11785−11793.
Marion, D., Ikura, M., Tschudin, R., & Bax, A. (1989) *J. Magn. Reson. 85*, 393−399.
Miller, E. C. (1978) *Cancer Res. 38*, 1479−1496.
Misra, B., & Amin, S. (1990) *J. Org. Chem. 55*, 4478−4480.
Mohamadi, F., Richards, N. G. J., Guida, W. C., Guida, R., Liscamp, R., Caufield, C., Chang, G., Hendrickson, T., & Still, W. C. (1990) *J. Comput. Chem. 11*, 440−467.
Neidle, S., Subbiah, A., Kuroda, R., & Cooper, C. S. (1982) *Cancer Res. 42*, 3766−3768.
Norman, D., Abuaf, P., Hingerty, B. E., Live, D., Grunberger, D., Broyde, S., & Patel, D. J. (1989) *Biochemistry 28*, 7462−7476.
Patel, D. J., Kozlowski, S. A., Nordheim, A., & Rich, A. (1982) *Proc. Natl. Acad. Sci. U.S.A. 79*, 1413−1417.
Pruess-Schwartz, F., Baird, W. M., Yagi, H., Jerina, D. M. Pigott, M. A., & Dipple, A. (1987) *Cancer Res. 47*, 4032−4037.
Razzel, W. E., & Khorana, H. G. (1961) *J. Biol. Chem. 236*, 1144−1149.
Reardon, D., Prakash, A. S., Hilton, B. D., Roman, J. M., Pataki, J., Harvey, R. G., & Dipple, A. (1987) *Carcinogenesis 8*, 1317−1322.
Schlick, T., Hingerty, B. E., Peskin, C. S., Overton, M. L., & Broyde, S. (1990) in *Theoretical Chemistry and Molecular Biophysics* (Beveridge, D., & Lavery, R., Eds.) pp 39−58, Academic Press, New York.
Shibutani, S., Margulis, L. A., Geacintov, N. E., & Grollman, A. P. (1993) *Biochemistry 32*, 7531−7541.
Singer, B., & Grunberger, D. (1983) *Molecular Biology of Mutagens and Carcinogens*, Plenum Press, New York.
Singh, S. B., Hingerty, B. E., Singh, U. C., Greenberg, J. P., Geacintov, N. E., & Broyde, S. (1991) *Cancer Res. 51*, 3482−3492.
Sklenar, V., Miyashiro, H., Zon, G., Miles, H. T., & Bax, A. (1986) *FEBS Lett. 208*, 94−98.
Taylor, E. R., & Olson, W. K. (1983) *Biopolymers 22*, 2667−2702.
Thakker, D. R., Levin, W., Yagi, H., Yeh, H. J. C., Ryan, D. E., Thomas, P. E., Conney, A. H., & Jerina, D. M. (1986) *J. Biol. Chem. 261*, 5404−5413.
van de Ven, F. J., & Hilbers, C. W. (1988) *Eur. J. Biochem. 178*, 1−38.
Venkatachalam, S., & Wani, A. A. (1994) *Carcinogenesis 4*, 565−572.
Wise, S. A., Benner, B. A., Chesler, S. N., Hilpert, L. R., Vogt, C. R., & May, W. E. (1986) *Anal. Chem. 58*, 3067−3077.
Wood, A. W., Chang, R. L., Levin, W., Thakker, D. R., Yagi, H., Sayer, J. M., Jerina, D. M., & Conney, A. H. (1984) *Cancer Res. 44*, 2320−2324.
Yagi, H., Thakker, D. R., Ittah, M., Croisy-Delcey, M., & Jerina, D. M. (1983) *Tetrahedron Lett. 24*, 1349−1352.

BI941981T